The Astrophysical Journal, 815:40 (9pp), 2015 December 10 doi:10.1088/0004-637X/815/1/40

DETECTION OF MOLECULAR GAS IN VOID GALAXIES: IMPLICATIONS FOR STAR FORMATION IN ISOLATED ENVIRONMENTS

M. Das[1], T. Saito[2], D. Iono[3], M. Honey[1], and S. Ramya[4]
[1] Indian Institute of Astrophysics, Bangalore, India; mousumi@iiap.res.in
[2] Department of Astronomy, Graduate school of Science, The University of Tokyo, 7-3-1 Hongo, Bunkyo-ku, Tokyo 133-0033, Japan
[3] Chile Observatory, NAOJ, Japan
[4] Shanghai Astronomical Observatory, Shanghai, China
Received 2015 July 6; accepted 2015 October 20; published 2015 December 7

ABSTRACT

We present the detection of molecular gas from galaxies located in nearby voids using the CO(1–0) line emission as a tracer. The observations were performed using the 45 m single dish radio telescope of the Nobeyama Radio Observatory. Void galaxies lie in the most underdense parts of our universe and a significant fraction of them are gas rich, late-type spiral galaxies. Although isolated, they have ongoing star formation but appear to be slowly evolving compared to galaxies in denser environments. Not much is known about their star formation properties or cold gas content. In this study, we searched for molecular gas in five void galaxies. The galaxies were selected based on their relatively high *IRAS* fluxes or Hα line luminosities, both of which signify ongoing star formation. All five galaxies appear to be isolated and two lie within the Bootes void. We detected CO(1–0) emission from four of the five galaxies in our sample and their molecular gas masses lie between 10^8 and 10^9 $M_\odot$. We conducted follow-up Hα imaging observations of three detected galaxies using the Himalayan Chandra Telescope and determined their star formation rates (SFRs) from their Hα fluxes. The SFR varies from 0.2 to 1 $M_\odot$ yr^{-1}; which is similar to that observed in local galaxies. Our study indicates that although void galaxies reside in underdense regions, their disks contain molecular gas and have SFRs similar to galaxies in denser environments. We discuss the implications of our results.

Key words: galaxies: evolution – galaxies: ISM – galaxies: spiral – galaxies: star formation – large-scale structure of universe – radio lines: ISM

1. INTRODUCTION

In the large-scale structure (LSS) of our universe, galaxies cluster along sheets, walls, and filaments leaving large empty regions called voids in between (Kirshner et al. 1981; Geller & Huchra 1989; Hoyle & Vogeley 2004; Foster & Nelson 2009; Sutter et al. 2012). They represent the most underdense parts of our universe and can vary in size, but typical values are 10–20 Mpc. For example, the nearby Local Void is ∼23 Mpc across (Tully et al. 2008), whereas the Bootes Void, which is the largest known void, is 60 Mpc across (Kirshner et al. 1987). In the past two decades, large optical surveys have revealed that voids contain a small but significant population of galaxies (Grogin & Geller 2000; Rojas et al. 2004; van de Weygaert et al. 2011). The smaller voids are mainly populated by small, gas rich, low surface brightness (LSB) dwarfs (Chengalur et al. 2015) and irregular galaxies (Karachentseva et al. 1999), but the larger voids also support a population of relatively bright galaxies that are late-type, gas rich systems that are often blue in color (Kreckel et al. 2011, 2015; Ricciardelli et al. 2014). This contradicts cold dark matter (CDM) models of structure formation where voids are predicted to be mainly populated by low luminosity galaxies (Peebles 2001). The presence of these blue void galaxies also indicates that there is ongoing star formation in voids. Even some early-type elliptical (E) and lenticular (S0) void galaxies (which are mainly composed of old stars) are found to be relatively blue in color (Wegner & Grogin 2008). However, although a signicant fraction of void galaxies do show star formation, they are generally evolving at a slower rate than galaxies in denser environments. This is evident from the color magnitude plot of these galaxies, in which the majority lie in the blue cloud region and not in the red region which is expected from an evolved galaxy population (Kreckel et al. 2012).

One of the main attractions of studying void galaxies is that they provide us with an opportunity to study star formation in isolated environments. It is not clear what drives star formation activity in such underdense environments. In denser parts of the universe, galaxy interactions and mergers play an important role in triggering star formation in gas rich galaxies. The interactions perturb the axisymmetric structure of the galaxy disks leading to enhanced cloud collisions, star formation, and gas infall to the nuclear regions. The enhanced nuclear gas surface densities can lead to nuclear star formation, active galactic nucleus (AGN) activity, and outflows. This cycle of activity ultimately results in bulge growth and the overall evolution of galaxies from small, star-forming blue systems to the more evolved red galaxies. In voids, galaxy interactions (such as the galaxy pair CG 693-692) are rare. Some void galaxies have low luminosity companions such as LSB dwarfs and dwarf spheroidals that are not easy to spot in optical images but nevertheless perturb galaxy disks and trigger star formation. Such interactions are difficult to detect in optical surveys. One way of detecting them is through HI surveys (e.g., Szomoru et al. 1996) where they may appear to have disturbed HI morphologies. Although some void galaxies do show such features in their HI contours (e.g., BHI 1514 +5155), interactions with visible or under-luminous companions are not high enough to explain the whole picture of star formation in voids, and thus interactions may not be the main driver of star formation activity in these underdense environments (Grogin & Geller 2000). Another possible driver of star formation activity in voids could be the slow accretion

Table 1
Sample Galaxies Observed in CO(1–0) Emisison with NRO

Galaxy Name	R.A. (J2000)	decl. (J2000)	D_L[c] (Mpc)	Redshift (z)	Type	Diameter ($''$)	g Magnitude	Void Name
SBS 1325+597	$13^h27^m18\overset{s}{.}6$	$+59^d30^m10^s$	70.4	0.016	Sm, H II	36.0 (k_s)	16.0	Ursa Minor I[b]
SDSS 143052[a]	$14^h30^m52\overset{s}{.}3$	$+55^d14^m40^s$	76.6	0.018	Extend.	76.0	19.5[d]	Ursa Minor I[b]
SDSS 153821[a]	$15^h38^m21\overset{s}{.}2$	$+33^d11^m05^s$	97.6	0.022	Sd	17.88 (r^d)	15.3	....
CG 598	$14^h59^m20\overset{s}{.}6$	$+42^d16^m10^s$	248.0	0.057	H II, Sbrst	44.7 (k_s)	16.4	Bootes
SBS 1428+529	$14^h30^m31\overset{s}{.}2$	$+52^d42^m26^s$	191.0	0.044	Sb, Sy 2	53.9 (k_s)	15.2	Bootes

Notes.
[a] SDSS 143052 full name is SDSS 143052.33+551440.0 1 and SDSS 153821 full name is SDSS 153821.22+331105.1.
[b] Void identifications for the first two galaxies were obtained from Kreckel et al. (2011).
[c] Distances for all galaxies were obtained from NED, except for that of SDSS 143052.33+551440.0 which was obtained from Kreckel et al. (2012).
[d] The optical size of the galaxy SDSS 143052.33+551440.0 1 was obtained from Kreckel et al. (2012) and for SDSS 153821.22+331105.1 from SDSS.

of cold gas by void galaxies from the intergalactic medium (IGM; Kreckel et al. 2012). Gas accretion can enhance the gas surface densities in disks. This can result in the formation of local disk instabilities which lead to disk star formation (Kereš et al. 2005; Dekel & Birnboim 2006). Recent observations of HI gas filaments connecting galaxies in voids suggests that this process may be important for galaxy pairs or small groups (Stanonik et al. 2009; Kreckel et al. 2012; Beygu et al. 2013).

Void galaxies are also one of the only probes by which we can investigate the void substructure—does it exist and how is it traced by galaxies? In ΛCDM theories of LSS formation, voids evolve with time into larger, emptier volumes. In the process, mass flows from voids into walls and filaments (Zel'dovich 1970; Icke 1984; Bond et al. 1996; Aragon-Calvo & Szalay 2013). Isolated or small groups of galaxies are left behind within the voids, formed by the compression of filaments or walls as the voids merge (Sahni et al. 1994; Sheth & van de Weygaert 2004; van de Weygaert et al. 2010). This void substructure, which in simulations appears as tenuous filaments and clusters of dark matter halos, can be traced by the distribution of void galaxies (Aragón-Calvo et al. 2007; Hahn et al. 2007; Cautun et al. 2014). Recent deep observations have shown that this void substructure exists (Alpaslan et al. 2014; Kreckel et al. 2012). However, only very deep surveys will reveal the inner structure of voids and how it connects the galaxies residing within the voids (Penny et al. 2015). As shown in simulations, there will also be gas flowing along these filaments and accreting onto the void galaxies. This can lead to star formation in the galaxy disks.

As a first step toward studying star formation and galaxy evolution in voids, we present a search for molecular gas in nearby void galaxies using the Nobeyama Radio telescope (NRO) with the CO(1–0) emission line as a tracer. Single dish observations will provide an estimate of the molecular gas masses, and the emission line profiles can reveal properties of the gas distribution, such as whether the gas is centrally concentrated or more extended in a rotating disk. There are only two earlier studies that have detected CO(1–0) in voids; we use those results to enhance our sample. We followed up our CO(1–0) detections with Hα observations of three detected galaxies and derived their SFRs. In the following sections, we describe our sample selection, the galaxy properties, observations, and results. For all distances, we have used $H_0 = 73\,\mathrm{km\,s^{-1}\,Mpc^{-1}}$ and $\Omega = 0.27$ (Komatsu et al. 2009).

2. SAMPLE SELECTION

We selected an initial sample of 12 galaxies from earlier studies of void galaxies (Weistrop et al. 1995; Szomoru et al. 1996; Cruzen et al. 2002) and the void galaxy survey (VGS) which used SDSS images to select a sample of 60 void galaxies and study their HI/radio properties using the WSRT telescope (Kreckel et al. 2012). Our short-listed galaxies had the following properties.

i. Significant HI gas masses and stellar masses greater than $10^9\,M_\odot$. This is to ensure that we avoid dwarf galaxies in our sample since previous studies of LSB dwarfs indicate that they are unlikely to have molecular gas (Das et al. 2006).
ii. Signatures of ongoing star formation. We checked the SDSS spectra of the sample galaxies to confirm the presence of emission lines that are typical of star formation (e.g., Hα, Hβ, and [O III]).
iii. For galaxies with *IRAS* fluxes, we selected only those that had $S_{100} > 1.0$ Jy.
iv. None of the galaxies had been previously studied in CO (1–0) emission.

However, due to unfavorable weather conditions, we were able to observe only five galaxies from this sample. These galaxies are listed in Table 1 and are briefly described below.

SBS 1325+597 (IRASF 13254+5945, VGS 34): This is a gas rich galaxy with a size of $D_{25} \sim 11.7$ kpc (Table 1) that has been studied as part of the VGS (Kreckel et al. 2011). The SDSS image of the galaxy shows a compact, red nucleus and a single, faint spiral arm. The SDSS optical spectrum has few emission lines suggesting only moderate star formation and shows no signatures of AGN activity. The HI is extended well beyond the optical radius and the outer isophotes are disturbed, which suggests that the galaxy may be interacting with a distant companion galaxy.
SDSS 143052.33+551440.0 (SDSS1430+5514, VGS 44): This is also a moderate-size disk galaxy with an r-band disk radius of ∼3.6 kpc and an HI radius of <7 kpc (Kreckel et al. 2012). There is no strong bulge or extended disk but the SDSS image reveals a blue nucleus that shows strong Hα emission in the optical spectrum, indicative of nuclear star formation.
SDSS 153821.22+331105.1 (SDSS1538+3311, VGS 57): This is the only galaxy in our sample that appears to have a bar. It has an extended disk of radius $17\overset{''}{.}9$ or ∼8.1 kpc in the SDSS r-band image and an HI radius of <9 kpc (Kreckel

Table 2
CO Emisison and Derived Gas Masses

Galaxy Name	t_{obs} (hr)	$S_{CO}\ \Delta v$ (K km s^{-1})	$L_{CO}(10^8)$ (K km s^{-1} pc^2)	H_2 Mass ($10^9\ M_\odot$)	Surface Density[b] ($\Sigma_{H_2}\ M_\odot$ pc^{-2})	HI Mass[c] ($10^9\ M_\odot$)	$\frac{M(H_2)}{M(HI)}$
SBS 1325+597	$1^h\ 12^m$	10.7 ± 0.2	(3.1 ± 0.1)	1.5 ± 0.03	12.4 ± 0.3	2.4 ± 0.3	0.6
SDSS 143052[a]	$1^h\ 16^m$	7.0 ± 0.2	(2.4 ± 0.1)	1.1 ± 0.03	27.5 ± 0.7	0.50 ± 0.1	2.3
SDSS 153821[a]	$1^h\ 31^m$	6.4 ± 0.2	(3.5 ± 0.1)	1.7 ± 0.05	29.9 ± 0.9	0.7 ± 0.2	2.5
CG 598	$2^h\ 26^m$	5.2 ± 0.1	(18.0 ± 0.3)	8.5 ± 0.1	3.8 ± 0.1	5.3 ± 0.8	1.6
SBS 1428+529	$0^h\ 25^m$	<0.6	<1.23	<0.6	....	2.0 ± 0.4	<0.4

Notes.
[a] SDSS 143052 full name is SDSS 143052.33+551440.0 1 and SDSS 153821 full name is SDSS 153821.22+331105.1.
[b] To derive the approximate molecular gas surface densities $\Sigma(H_2)$ we used the galaxy diameters and distances listed in Table 1.
[c] The HI masses for the galaxies SBS 1325+597 (VGS 34), SDSS 143052.33+551440.0 (VGS 44), and SDSS 153821.22+331105.1 (VGS 57) were obtained from Kreckel et al. (2012) and adjusted for the distances listed in Table 1. For CG 598 and SBS 1428+529 we used data from Szomoru et al. (1996).

et al. 2012). Though the galaxy is relatively blue and the SDSS nuclear spectrum shows strong Hα emission, other signatures of strong star formation such as [O I] emission, which is associated with shocks, are lacking. The ongoing star formation is located mainly along the bar.

CG 598 (IRAS F14575+4228): This is a distant but large galaxy in the Bootes void that has a disk radius of 22.″4 or ∼26.2 kpc in the k_s band and shows signs of strong star formation in its optical spectrum (e.g., Hα, Hβ, and [O II] emission; Cruzen et al. 2002). It is gas rich and the HI gas disk is extended well beyond the optical disk (Szomoru et al. 1996). In the SDSS *g*-band image, the galaxy appears to be accreting a smaller galaxy. The interaction probably triggered the burst of star formation.

SBS 1428+529 (IRAS F14288+5255): This is also a distant galaxy located in the Bootes void. Like CG 598 it is large in size (radius ∼27″ or ∼24.6 kpc) but appears to be isolated. It has a bright bulge, distinct spiral arms, and a strong bar. It is the only galaxy in our sample that shows AGN activity; it hosts a Seyfert 2-type nucleus (Cruzen et al. 2002).

3. CO OBSERVATIONS AND DATA REDUCTION

The $^{12}CO(J = 1 - 0)$ single dish emission line observations were performed using the 45 m Nobeyama Radio Telescope during the period 2013 April 14–25. At the CO rest frequency of 115.271204 GHz, the half-power beam width (HPBW) is 15″ and the main beam efficieny is 30%. We used the one beam (TZ1), dual polarization, sideband separating receiver (TZ). The signal was digitized to 3 bits before being transferred to the digital FX-type spectrometer SAM45, which has a bandwidth of 4 GHz (Nakajima et al. 2008). Typical system temperatures were 160–260 K. The chopper-wheel method was used for temperature calibration with a swtiching cycle of 10 s. The resultant output had 4096 channels and a frequency resolution of 488 kHz.

The on source time for the first four galaxies varied between 1 and 1.5 hr. Due to poor weather conditions, the fifth galaxy SBS 1428+529 was observed for only 25 minutes (Table 2). The pointing accuracy was about ∼2″ to ∼4″. The data was analyzed using the NRO calibration tool NEWSTAR. Data with a wind velocity greater than 5 km s^{-1} and data points with winding baselines were flagged out. The antenna temperature (T_A) was converted to the main beam temperature (T_{mb}) using a main beam efficiency of $\eta_b = 0.3$, where $T_A = T_{mb}/\eta_b$. The spectra were converted from Kelvin to Jansky using a conversion factor of 2.4 Jy K^{-1}.

4. Hα OPTICAL OBSERVATIONS AND DATA REDUCTION

We conducted Hα observations of three galaxies in our sample, SBS 1325+597, SDSS 143052.33+551440.0, and SDSS 153821.22+331105.1. The remaining two galaxies were not observed because we did not have suitable filters. The Hα observations were performed using the Himalayan Faint Object Spectrograph Camera (HFOSC) mounted on the 2 m Himalayan Chandra Telescope (HCT) installed at the Indian Astronomical Observatory (IAO), Hanle, India. HFOSC has a 2K × 4K SITe CCD chip with a plate scale of 0.296 arcsec pixel^{-1}. The central 2K × 2K covers a field of view of 10 × 10 arcmin^2. The observations were obtained on 2014 April 11 and 25. For the galaxies SBS 1325+597 and SDSS 143052.33+551440.0, we used the Hα broad filter with a bandwidth of ∼500 Å to obtain the Hα images. However, SDSS 153821.22+331105.1 is at a higher redshift of $z = 0.023$ and the Hα line is shifted to 6714 Å. Hence, for this galaxy, we used the narrowband [S II] filter of bandwidth ∼100 Å centered around the wavelength 6724 Å.

To obtain the continuum subtracted Hα, images we followed the procedure as outlined below. The galaxy images were obtained in both the broadband *r* filter and the narrowband filters centered around the Hα line. The bias frames and twilight flats were used for preprocessing of the images. The data reduction was done using the standard packages available in IRAF.[5] The frames were bias subtracted and flat field corrected using the master bias and master flat frames. The cosmic-ray hits were removed using the task COSMICRAYS in IRAF. The images of the two different filters were aligned geometrically using the tasks GEOMAP and GEOTRAN. The point-spread function (PSF) of both the broad- and narrowband frames were matched. The scale factor between the broadband *r* frame and the Hα frame was determined using the field stars. The continuum subtracted Hα images were obtained by subtracting the PSF-matched scaled continuum *r*-band images from the narrowband images as described in Waller (1990). Flux calibration was done using the spectrophotometric

[5] Image Reduction and Analysis Facility Software distributed by National Optical Astronomy Observatories, which are operated by the Association of Universities for Research in Astronomy, Inc., under cooperative agreement with the National Science Foundation.

Table 3
Hα Luminosities, Star Formation Rates and Star Formation Thresholds

Galaxy Name	Hα Flux (10^{-14} erg cm^{-2} s^{-1})	Hα Luminosity (10^{40} erg s^{-1})	SFR ($M_\odot$ yr^{-1})	SFE[b]	M(HI + H_2) (10^9 $M_\odot$)	Disk Rotation (km s^{-1})	$\frac{\Sigma(\mathrm{HI}+\mathrm{H_2})}{\Sigma_{\mathrm{crit}}}$[c]
SBS 1325+597	4.44	2.49	0.20	0.03	3.89	116.30	2.7
SDSS 143052[a]	11.65	7.61	0.60	0.21	1.60	145.62	1.5
SDSS 153821[a]	11.94	1.29	1.02	0.05	2.35	200.0	1.4
CG 598	....	...	1.48[d]	...	13.85	...	...
SBS 1428+529	5.65[e]	23.3	1.85	....	<2.61	...	...

Notes.
[a] SDSS 143052 full name is SDSS 143052.33+551440.0 1 and SDSS 153821 full name is SDSS 153821.22+331105.1.
[b] The star formation efficiency (SFE) is defined as the SFR divided by the ratio of molecular gas mass to disk rotation timescales (see Section 5 for details).
[c] This is the ratio of the total gas surface density and the critical surface density for star formation $\Sigma(\mathrm{HI}+\mathrm{H_2})/\Sigma_{\mathrm{crit}} > 1$ in star-forming galaxies (Kennicutt 1998). Its calculation is discussed in Section 5.
[d] The star formation rate (SFR) is derived from the UV flux (Sargsyan & Weedman 2009).
[e] The Hα flux for SBS 1428+529 is from Weistrop et al. (1995).

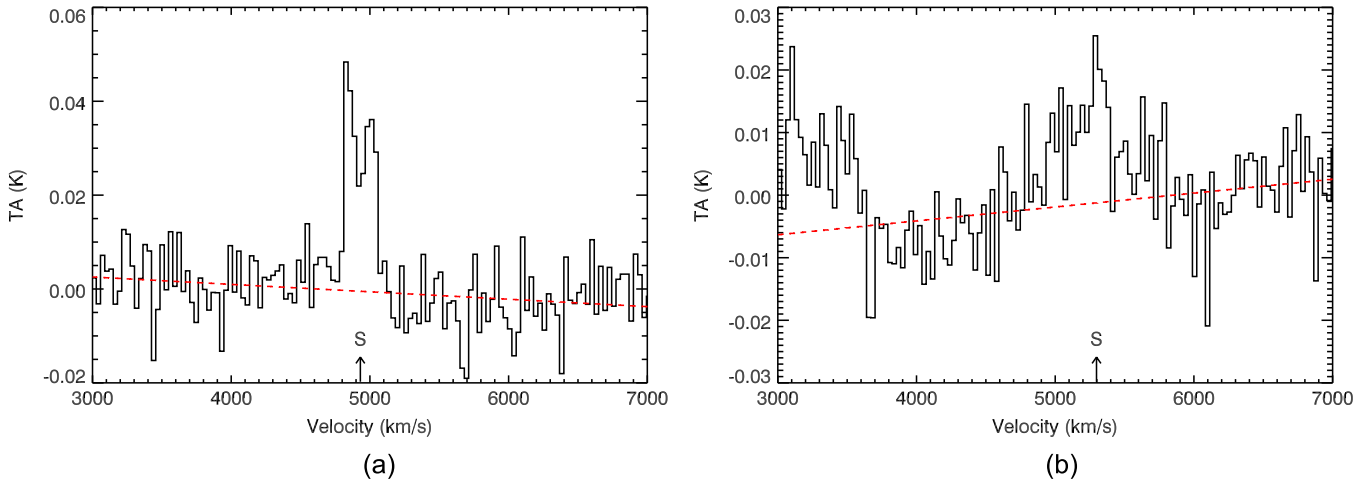

Figure 1. (a) CO(1–0) spectrum observed from the galaxy SBS 1325+597. The emission line has a clear double-horned profile. The dashed line in red represents the baseleine fitted to the spectrum. The systemic velocity of the galaxy, $v_{\mathrm{sys}} = 4917$ km s^{-1} (Kreckel et al. 2012) is marked with an "S" and an arrow on the velocity axis. It lies in between the two emission peaks. This indicates that the molecular gas is in a rotating disk. (b) CO(1–0) spectrum from the galaxy SDSSJ 143052.33 +551440.0. The fitted baseline is marked with a dashed red line and the systemic velocity of the galaxy, $v_{\mathrm{sys}} = 5295$ km s^{-1} (Kreckel et al. 2012) is marked. The emission can be clearly distinguished but is distributed over a range of velocities which suggests that the molecular gas distribution may not be centrally concentrated in the nucleus.

standard star HZ44 (Oke 1990). Flux calibrated continuum subtracted Hα images are shown in Figures 3–5.

5. RESULTS

In this section, we discuss our molecular gas detections (Table 1), follow-up Hα observations for three of the detected galaxies (Table 3), and the implications of our results.

5.1. CO(1–0) Detections

We have detected ^{12}CO($J = 1 - 0$) emission from four of the five sample galaxies that we observed and the fluxes are listed in Table 2. The non-detection in SBS 1428+529 could be due to the short duration of the scan, which was limited by bad weather. The noise of the spectrum is 0.0024 K. Assuming a typical CO(1–0) bandwidth of 250 km s^{-1}, we obtain $I_{\mathrm{CO}} <$ 0.6 K km s^{-1}, which gives a limiting molecular gas mass of $0.59 \times 10^9\ M_\odot$ (Table 2). Of the four detections, SBS 1325 +597 has the most striking line profile; it has a double-horned structure indicating a rotating disk of molecular gas (Figure 1(a)). The velocity separation of the peaks is ~200 km s^{-1}. Assuming a disk inclination of 59°.3 (Makarov et al. 2014)[6], the disk rotation is 116 km s^{-1}. This is similar to the HI rotation speed in this galaxy derived from the HI observations of Kreckel et al. (2012). In SDSS 143052.33 +551440.0 (Figure 1(b)), the CO line profile is fairly symmetric about the central systemic velocity of the galaxy but is distributed over a range of velocities which suggests that the molecular gas probably extends over the galaxy disk rather than being concentrated within the nucleus. In both SDSS 153821.22+331105.1 and CG 598, the molecular gas is centrally peaked (Figures 1(d) and 2(b)). SDSS 153821.22 +331105.1 is barred, and hence the molecular gas may have been driven into the center by the bar (Sakamoto et al. 1999).

5.2. Molecular Gas Masses and Surface Densities

The CO fluxes in K km s^{-1} were converted to Jy km s^{-1} using a conversion factor (Jy K^{-1}) of 2.4. The CO line luminosity was determined using the relation $L_{\mathrm{CO}} = 3.25 \times 10^7$

[6] http://leda.univ-lyon1.fr/

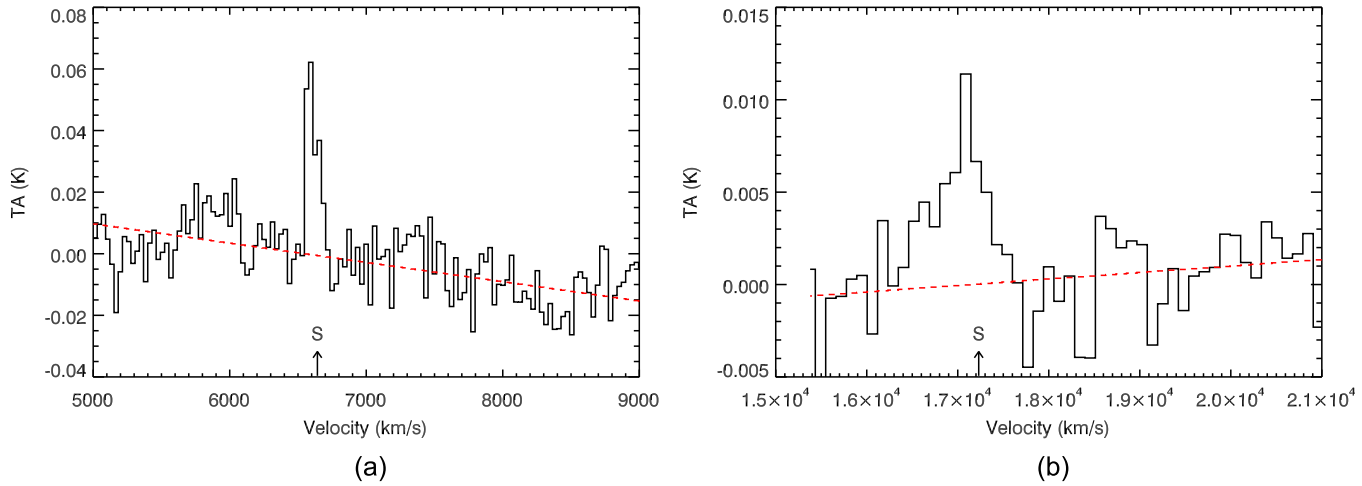

Figure 2. (a) CO(1–0) spectrum of the galaxy SDSS 153821.22+331105.1. The emission is peaked about the systemic velocity of the galaxy, $v_{sys} = 6630$ km s^{-1} (Kreckel et al. 2012), which suggests that the gas is concentrated in the center of the galaxy. The fitted baseline is marked with a dashed red line. (b) CO(1–0) spectrum observed from CG 598. The gas distribution is also symmetric about the center of the galaxy, which is marked at $v_{sys} = 17{,}226$ km s^{-1} (NED value) with an "S."

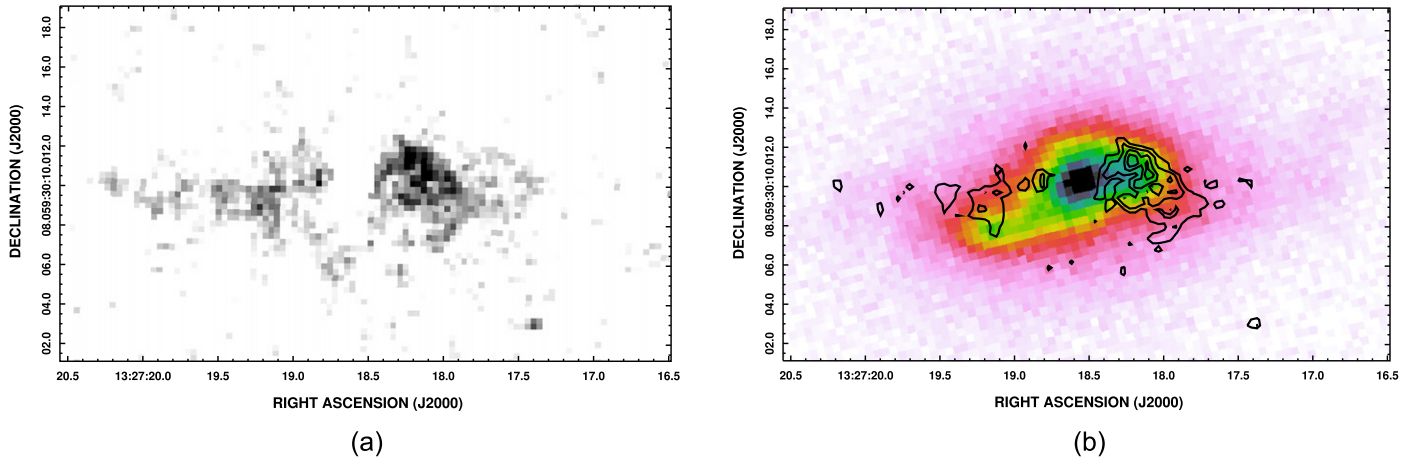

Figure 3. (a) Sky subtracted Hα image of SBS 1325+597. The Hα emission is diffuse and distributed on either side of the nucleus. There appears to be more star formation west of the nucleus. (b) Contours of the Hα emission superimposed on the SDSS g-band image of the galaxy. The contour levels are 0, 0.12, 0.18, 0.24, and 0.30, where the units are in counts s^{-1} and the sky subtracted background has a noise level of approximately 0.03. The emission has a ringlike morphology and is associated with the disk.

$(S_{CO}\Delta V/\mathrm{Jy\ km\ s^{-1}})\ \ (D_L/\mathrm{Mpc})^2(\nu_{res})^{-2}(1+z)^{-1}$ and the molecular gas masses were estimated using the relation $M(\mathrm{H_2}) = [4.8L_{CO}(\mathrm{K\ km\ s^{-1}})]$ (Solomon & van den Bout 2005). The molecular gas masses lie in the range (1–8) $\times$ 10^9 $M_\odot$ (Table 2) which is comparable to the molecular gas masses observed in nearby bright galaxies that lie in denser environments (Helfer et al. 2003). Using the 2MASS galaxy sizes, we estimated the suface densities Σ of the molecular gas distribution; it lies in the range (3.8–30) $M_\odot\,\mathrm{pc}^{-2}$ (Table 3), which is also similar to that observed in nearby bright galaxies (Kennicutt 1998). Thus, both the molecular gas masses and gas surface densitites are not unusually low, even though the galaxies are in low-density environments.

5.3. Hα Imaging and SFRs

As mentioned earlier, due to a lack of suitable filters, we were only able to do Hα imaging of three galaxies in our sample, SBS 1325+597, SDSS 143052.33+551440.0, and SDSS 153821.22+331105.1 (Figures 3–5).

i. In SBS 1325+597, the Hα emisison is distributed over two regions on either side of the galaxy center, which indicates that it is only associated with the inner disk of the galaxy (Figure 3). This distribution agrees well with the CO(1–0) emission profile (Figure 1), which is double horned about the systemic velocity of the galaxy and indicates that the molecular gas is also distributed in a ring or torus about the galaxy center. In the SDSS optical image, it is clear that the galaxy has a red bulge but a bluish star-forming disk. The Hα luminosity gives a moderate SFR of 0.2 $M_\odot\,\mathrm{yr}^{-1}$ (Table 3). The galaxy also shows extended UV emission in its *GALEX* image. The emission peak is offcenter from the nucleus and located east of the nucleus. Thus, the overall picture of this galaxy is that of an isolated void galaxy with a moderately star-forming disk that is rich in molecular gas.
ii. SDSS 143052.33+551440.0 is a small galaxy with a bright nucleus that appears blue in its SDSS optical image. The Hα emisison peaks close to the center of the galaxy but is extended over the enitire disk (Figure 4). The Hα luminosity gives an SFR of 0.6 $M_\odot\,\mathrm{yr}^{-1}$

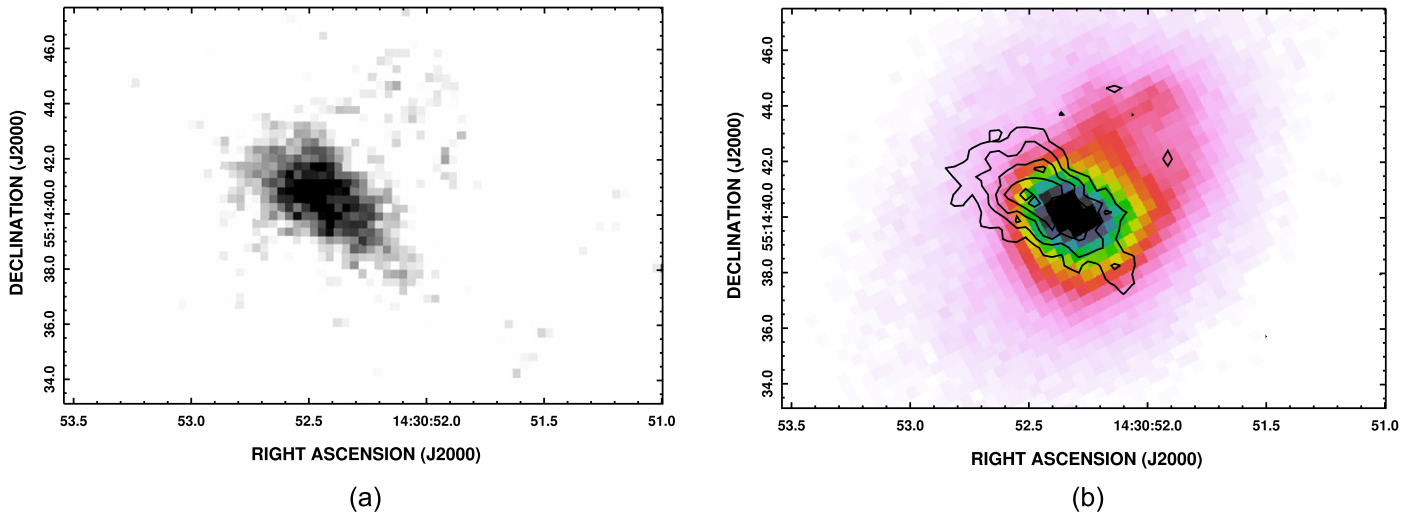

Figure 4. (a) Sky subtracted Hα image of SDSS 143052.33+551440.0. The Hα emission is distributed over the galaxy and extended on one side. There is also diffuse emission lying to the northwest of the galaxy center that matches diffuse emission in the *g*-band image as well. (b) Contours of Hα emission superimposed on the SDSS *g*-band image of the galaxy. The contour levels are 0.27, 0.45, 0.63, 0.81, and 0.99, where the units are in counts s^{-1} and the sky subtracted background has a noise level of approximately 0.09. The Hα contours are extended on one side of the nucleus.

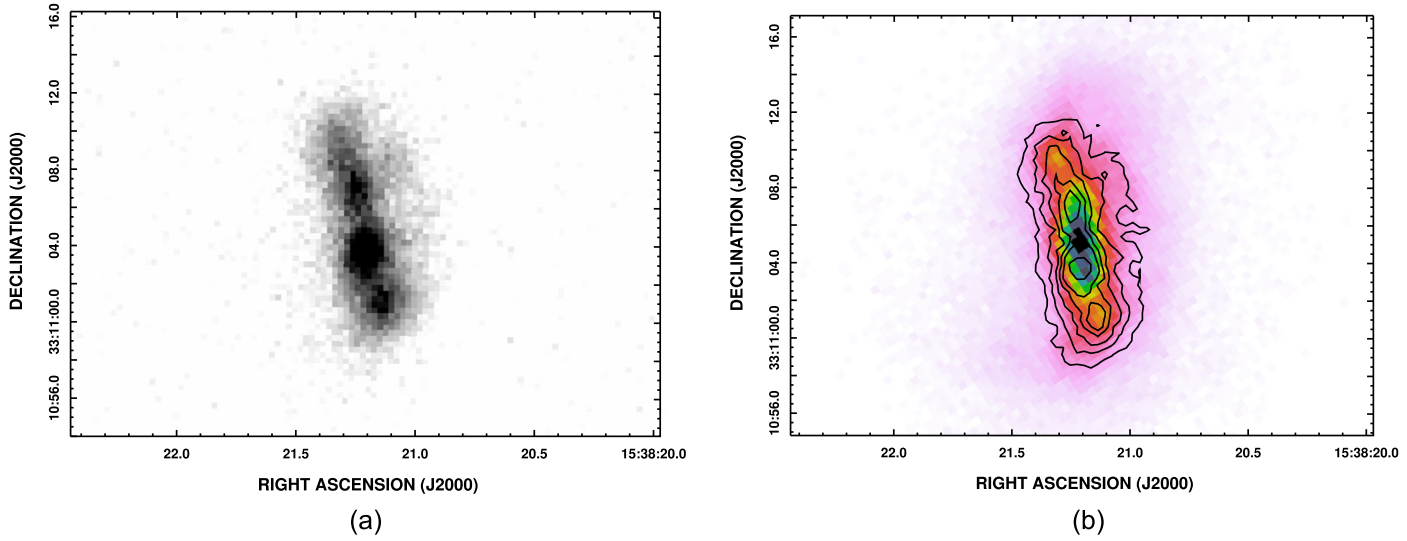

Figure 5. (a) Hα image of SDSS 153821.22+331105.1. The emission is strong and distributed along the bar in the galaxy. The flux density is highest in the nucleus and distributed over two regions along the bar. (b) Contours of Hα emission superimposed on the SDSS *g*-band image of the galaxy. The contour levels are 0.27, 0.45, 0.63, 0.81, and 0.99, where the units are in counts s^{-1} and the sky subtracted background has a noise level of approximately 0.02. There is clearly strong star formation along the bar. The emission peaks on either side of the nucleus.

(Table 3) which is relatively strong for a galaxy of this size. Both the Hα flux and the CO line emission appear to peak offcenter from the nucleus. The *GALEX* NUV emission is also extended over the galaxy. Thus, SDSS 143052.33+551440.0 is a small, star-forming, gas-rich galaxy.

iii. SDSS 153821.22+331105.1 is the only barred galaxy in our sample. It appears to be an isolated, blue, star-forming galaxy with a small bulge and faint spiral arms associated with the bar (Figure 5). The Hα emission peaks in the nucleus and is extended over the entire bar. This is similar to the molecular gas distribution which is sharply peaked about the systemic velocity of the galaxy (Figure 3) indicating that the molecular gas is concentrated in the center of the galaxy. It may have been driven into the nucleus by the bar. The bar may also have triggered the star formation. There is not much Hα emission detected from the disk but the total Hα luminosity gives a relatively high SFR of 1.02 $M_{\odot}$ yr^{-1} (Table 3), probably due to the large Hα luminosity (i.e., SFR) along the bar. There is no *GALEX* image for this galaxy. Thus, SDSS 153821.22+331105.1 appears to be a moderate-sized barred galaxy that has strong star formation associated with the bar. It is a good example of ongoing secular evolution in a void galaxy where the nuclear star formation contributes to bulge growth and the gas evolution is probably driven by the bar.

5.4. Star Formation Efficiency and the Critical Mass Surface Density for Star Formation

The star formation efficiecy (SFE) is defined as the SFR divided by the ratio of the molecular gas mass to the dynamical or disk rotation timescales (Silk & Mamon 2012). This is an

Table 4
Comparison of Molecular Gas Detection in Other Void Galaxies

Galaxy Name	Distance (Mpc)	H_2 Mass ($10^9\ M_\odot$)	HI Mass ($10^9\ M_\odot$)	$\frac{M(H_2)}{M(HI)}$	SFR ($M_\odot\ yr^{-1}$)	Reference
CG 910	188	4.2	....	....	...	Sage et al. (1997)
CG 684	204	4.7	9.2	0.51	1.83[a]	Sage et al. (1997), Szomoru et al. (1997)
VGS 31b (Mrk 1477)	69	1.3[b]	1.5	0.92	0.49[c]	Beygu et al. (2013)

Notes.
[a] The SFR was derived from the Hα line flux $I = 4.91 \times 10^{-14}$ erg cm^{-2} s^{-1} (Peimbert & Torres-Peimbert 1992) using the relation SFR $= L(H\alpha)/1.26 \times 10^{42}$ (Kennicutt et al. 1998).
[b] We have used the L_{CO}' from Beygu et al. (2013) and the relation $M(H_2) = 4.8\ L_{CO}'$ to determine this value.
[c] The SFR was derived from the SDSS DR10 Hα line flux of $I = 11.56 \times 10^{-14}$ erg cm^{-2} s^{-1}.

important quantity to determine as it indicates what fraction of the molecular gas is converted into stars during star formation in a galaxy and the gas depletion timescales (Leroy et al. 2008). We estimated the approximate disk rotation timescales from the HI position velocity (PV) plots in Kreckel et al. (2012) using the flat rotation velocities v and HI extent r(HI). We have derived the SFE in three galaxies (Table 3). For the remaining two galaxies, disk rotation velocities were not available in the literature, and hence we could not derive their SFEs. We used the relation SFE $= \mathrm{SFR}/M(H_2) \times \frac{2\pi\ r}{v}$, which becomes $\frac{\mathrm{SFR}}{M(H_2)}\frac{D''}{v\,(\mathrm{km\ s^{-1}})}(D_{\mathrm{Mpc}})$, where $M(H_2)$ is the molecular gas mass in solar mass units, v is the depojected rotation velocities (i.e., $v_{obs}/\mathrm{Sin}\ i$), D'' is the galaxy diameter in arcseconds, and D_{Mpc} is the galaxy distance in Mpc. Of the three galaxies, SDSS 143052.33+551440.0 has the highest SFE, probably because it is much smaller than the other two galaxies and yet has comparable SFRs. It is also very blue in its SDSS composite image, which suggests a high SFR. We have also calculated the critical surface density for star formation (Σ_{crit}; Kennicutt 1989) again using the approximate disk rotation velocities and total gas surface densities $\Sigma(\mathrm{HI} + H_2)$, where $\Sigma_{\mathrm{crit}} = \alpha\kappa\sigma_{\mathrm{gas}}/3.36$ G. We assumed $\kappa = \sqrt{2}\,v/r$, $\alpha = 0.69$, $\sigma_{\mathrm{gas}} = 10\ \mathrm{km\ s^{-1}}$, where v is the disk rotation velocity. For $\Sigma/\Sigma_{\mathrm{crit}} > 1$, the disk is unstable. Table 3 shows that all three star-forming galaxies have gas surface densitites above the critical threshold. This is in contrast to LSB galaxies that have large HI masses but diffuse stellar disks that do not support star formation (Das et al. 2010).

6. COMPARISON WITH PREVIOUS CO DETECTIONS

There are only two other studies of molecular gas in void galaxies (Sage et al. 1997; Beygu et al. 2013). In the earlier study by Sage et al., CO(1–0) was detected from four galaxies lying within the Bootes void. Of these four galaxies, two galaxies, CG 910 and CG 684, show strong CO emission centered around their systemic velocities. We have adjusted the distances to $H_o = 73\ \mathrm{km\ s^{-1}\ Mpc^{-1}}$ and recalculated the molecular gas masses (Table 4). Both galaxies have molecular gas masses of the order of $10^9\ M_\odot$, which is similar to that observed in our sample galaxies. CG 910 is an isolated galaxy with a relatively high disk inclination (56°.2) and a red bulge. It has a double-horned CO(1–0) emission line profile with peaks separated by $\sim$370 km s^{-1}, which indicates that the molecular gas disk is rotating with velocity $v_r = 223\ \mathrm{km\ s^{-1}}$. The SDSS DR6 nuclear spectrum shows only weak Hα emisison which indicates that there is only moderate star formation in this galaxy. The other galaxy, CG 684, is closely interacting with a companion galaxy (Szomoru et al. 1996). The blue color of its SDSS optical composite image suggests ongoing star formation (Cruzen et al. 2002) that was probably triggered by a close tidal interaction with a companion galaxy. The CO(1–0) emission line has two broad peaks separated by $\sim$710 km s^{-1}, which is too large to be due to disk rotation. Instead, the two peaks probably represent gas disks in CG 684 and its companion galaxy. The strong Hα emission line in the SDSS (DR6) spectra of CG 684 indicates that there is ongoing nuclear star formation (Table 4).

The second study by Beygu et al. detected CO emission in the star-forming galaxy Mrk 1477, which is denoted by VGS 31b in their VGS (Kreckel et al. 2012). The galaxy is part of a string of three galaxies that appear to lie along an HI filament in a void. Mrk 1477 is clearly tidally interacting with the nearest galaxy, VGS 31a, and has a bar as well as ring in its disk. Of the three galaxies, only Mrk 1477 was studied in CO emission and the molecular gas mass is similar to our detections (Table 4). Unlike SBS 1325+597 or CG 910, Mrk 1477 does not have a double-horned CO(1–0) profile. Instead, the molecular gas appears to be piled in the center of the disk. It has probably been driven into the galaxy center by the bar which shows strong streaming motion in Hα (Beygu et al. 2013). The nuclear SFR is significant and has a value of 0.45 $M_\odot\ \mathrm{yr^{-1}}$ (Table 4); the nucleus appears to be blue in the optical SDSS image of the galaxy.

Thus, to date, including our detections there are seven galaxies detected in CO emission. Their molecular gas masses lie in range 10^8–$10^9\ M_\odot$ for g-band absolute magnitudes 14.8–19 and SFRs 0.2–1.85. Also, of the seven galaxies detected in CO emission, five have blue bulges or inner disks indicating ongoing nuclear star formation. The two exceptions are CG 910 and SBS 1325+597, both of which have red bulges in their (composite) SDSS images. However, it is interesting to note that both CG 910 and SBS 1325+597 have double-horned CO(1–0) emission profiles, which shows that their molecular gas is distributed mainly in their disks and probably associated with disk star formation rather than nuclear star formation. The ongoing disk star formation in SBS 1325 +597 is indicated by the faint blue color and the Hα emission from its disk (Figure 3). A drawback of our work is that our sample is small, even when previous detections of molecular gas are included (Table 4), and biased toward blue galaxies. Hence, it is not representative of the entire range of void galaxies and there is also no control sample. However, when we take into account the significant amount of star formation

observed in void galaxies (e.g., Kreckel et al. 2012), it is probably safe to state that molecular gas is not rare in voids.

7. DISCUSSION

Since molecular gas requires dust to form, its presence also indicates that there have been several cycles of star formation in these galaxies. In this section, we address the following questions. (a) What drives star formation in these underdense environments and (b) are void galaxies dark matter dominated systems?

i. *Galaxies and the void substructure:* Void galaxies form from the rare, small-scale peaks in the primordial density field and a larger volume will likely include more of these peaks. However, void galaxies may also form within the void substructure. In the hierarchical picture of void evolution, smaller voids merge to form larger voids (Sheth & van de Weygaert 2004) causing mass to flow from the void centers to the surounding walls (Aragón-Calvo et al. 2007; Hahn et al. 2007; Aragon-Calvo & Szalay 2013). In the process, some matter may be left behind within the voids as filaments and mini-walls tracing a void substructure (Dubinski et al. 1993; Sahni et al. 1994). In this scenerio, small groups of galaxies can form within voids at places where the filaments or sheets intersect each other. So even though the large-scale environemnt in voids is sparse, galaxy pairs (e.g., CG 692-CG 693) or small groups (e.g., VGS 31a,b,c) can form within the void substructure. There is now evidence that such filamentary structures within voids exist (Popescu et al. 1996; Beygu et al. 2013; Alpaslan et al. 2014). These galaxies interact or merge giving rise to star formation. Thus, some of the star formation that we observe in voids could be driven by the expansion and merging of the voids themselves. Thus, it is possible that we may observe more star-forming galaxies and interacting systems in the larger voids, such as the Bootes void (Szomoru et al. 1996) where many more voids could have merged to form a larger void.

ii. *Slow gas accretion onto void galaxies from the IGM:* Slow, cold gas accretion by galaxies along filaments has been shown to be important for galaxies with relatively low-mass halos (Kereš et al. 2005; Dekel & Birnboim 2006; Bouché et al. 2010). In void galaxies, cold gas from the intergalactic medium (IGM) may be accreted along the filaments that form part of the void substructure. The gas accretion increases the gas surface density and cools the disks. This can result in the formation of local disk instabilities that can trigger star formation. Cooler disks are also more prone to bar instabilities which can again trigger star formation (e.g., SDSS 153821.22 +331105.1; Sellwood & Wilkinson 1993).

iii. *Are voids dominated by LSB galaxies?:* ΛCDM models of structure formation predict that voids are populated mainly by dark matter dominated galaxies, similar to the LSB galaxies that are observed at low redshifts (Peebles & Nusser 2010). Although the smaller voids such as the Local Void, have a significant population of LSB dwarfs, the number density is not as high as predicted. Instead, surprisingly, voids contain a significant population of blue galaxies (Peebles 2001). The main characterstics of LSB galaxies are their extended HI gas disks and low to moderate SFRs. Molecular gas is very rare in these galaxies (Das et al. 2006) and their dust content is low (Rahman et al. 2007). Our study clearly shows that molecular gas is fairly abundant in void galaxies and star formation is also present. This suggests that voids are probably not dominated by LSB galaxies.

iv. *The dark matter content of SBS 1325+597 (VGS 34):* This galaxy is the only one in our sample that has an HI PV plot that is extended enough to determine the flat rotation velocity in the galaxy disk. The double-horned CO emission profile (Figure 1(a)) and the PV plot in Kreckel et al. (2012) indicate a projected flat disk velocity of 100 km s^{-1}, which when deprojected with an inclination angle of 59°.3 gives a disk rotation velocity of $v_c = 116.3$ km s^{-1}. We used this velocity to obtain an approximate estimate of the dynamical mass. The PV plot contours extend out to an approximate radius of 30″ which correponds to a lengthscale of 9.9 kpc, where 1″ = 330 pc. Thus, the dynamical mass is $M_{\rm dyn} = 3.01 \times 10^{10}\,M_{\odot}$. To derive the stellar mass, we used the $(M/L)_k$ ratios derived from closed box models of chemical evolution (Bell & de Jong 2001), where $\log(M/L) = a_k + b_k(B-V)$. Using the $(g-r)$ magnitudes from SDSS DR12 and a conversion formula of $(B-V) = 0.98(g-r) + 0.22$ (Jester et al. 2005), we obtained a value of $(M/L)_k = 1.07$. Using the 2MASS total flux for this galaxy, we obtained a stellar mass of $M_* = 1.27 \times 10^{10}\,M_{\odot}$ for SBS 1325+597. As listed in Table 2, $M(\mathrm{HI+H_2}) = 3.84 \times 10^9\,M_{\odot}$. Hence, the baryonic mass is 0.55 of the total dynamical mass and so the galaxy is not dark matter dominated. Although this is one isolated case, the result may apply to other star-forming galaxies in voids. Similar studies of a larger and more varied sample of void galaxies are necessary to determine the dark matter content of these galaxies.

8. CONCLUSIONS

i. We searched for molecular gas in a sample of five void galaxies using the CO(1–0) emission line. We detected molecular gas in four of the five observed galaxies. The molecular gas masses lie in the range 10^8–$10^9\,M_{\odot}$.

ii. We performed follow-up Hα imaging observations of three of the detected galaxies and determined their SFRs from their Hα fluxes. The SFR varies from 0.2 to 1 $M_{\odot}$ yr^{-1}, which is similar to that observed in nearby star-forming galaxies.

iii. Our study and two others in the literature indicate that although void galaxies reside in underdense regions, their disks contain molecular gas and may have star formation properties similar to galaxies in denser environments.

iv. We derived the baryonic and dark matter content of one of our sample galaxies, SBS 1325+597. We find that its baryonic content is 0.55 of the total dynamical mass, and hence is not dark matter dominated. The result may apply to other star-forming galaxies in voids.

M.D. thanks the anonymous referee for very useful comments that improved the paper. T.S. is financially supported by a Research Fellowship from the Japan Society for the Promotion of Science for Young Scientists. S.R. kindly acknowledges the award of NSFC (grant No. 11450110401)

and the President's International Fellowship Initiative (PIFI) awarded by the Chinese Academy of Sciences. This work was based on observations at the Nobeyama Radio Observatory (NRO). NRO is a branch of the National Astronomical Observatory of Japan, National Institutes of Natural Sciences. The optical observations were done at the Indian Optical Observatory (IAO) at Hanle. We thank the staff of IAO, Hanle, and CREST, Hosakote, that made these obervations possible. The facilities at IAO and CREST are operated by the Indian Institute of Astrophysics, Bangalore. This research has made use of the NASA/IPAC Extragalactic Database (NED), which is operated by the Jet Propulsion Laboratory, California Institute of Technology, under contract with the National Aeronautics and Space Administration. Our work has also used SDSS-III data. Funding for SDSS-III has been provided by the Alfred P. Sloan Foundation, the Participating Institutions, the National Science Foundation, and the U.S. Department of Energy Office of Science. The SDSS-III web site is http://www.sdss3.org/. SDSS-III is managed by the Astrophysical Research Consortium for the Participating Institutions of the SDSS-III Collaboration including the University of Arizona, the Brazilian Participation Group, Brookhaven National Laboratory, Carnegie Mellon University, University of Florida, the French Participation Group, the German Participation Group, Harvard University, the Instituto de Astrofisica de Canarias, the Michigan State/Notre Dame/JINA Participation Group, Johns Hopkins University, Lawrence Berkeley National Laboratory, Max Planck Institute for Astrophysics, Max Planck Institute for Extraterrestrial Physics, New Mexico State University, New York University, Ohio State University, Pennsylvania State University, University of Portsmouth, Princeton University, the Spanish Participation Group, University of Tokyo, University of Utah, Vanderbilt University, University of Virginia, University of Washington, and Yale University.

Facilities: No:45m, Himalayan Chandra Telescope, Sloan.

REFERENCES

Alpaslan, M., Robotham, A. S. G., Obreschkow, D., et al. 2014, MNRAS, 440, L106
Aragón-Calvo, M. A., Jones, B. J. T., van de Weygaert, R., & van der Hulst, J. M. 2007, A&A, 474, 315
Aragon-Calvo, M. A., & Szalay, A. S. 2013, MNRAS, 428, 3409
Bell, E. F., & de Jong, R. S. 2001, ApJ, 550, 212
Beygu, B., Kreckel, K., van de Weygaert, R., van der Hulst, J. M., & van Gorkom, J. H. 2013, AJ, 145, 120
Bond, J. R., Kofman, L., & Pogosyan, D. 1996, Natur, 380, 603
Bouché, N., Dekel, A., Genzel, R., et al. 2010, ApJ, 718, 1001
Cautun, M., van de Weygaert, R., Jones, B. J. T., & Frenk, C. S. 2014, MNRAS, 441, 2923
Chengalur, J. N., Pustilnik, S. A., Makarov, D. I., et al. 2015, MNRAS, 448, 1634
Cruzen, S., Wehr, T., Weistrop, D., Angione, R. J., & Hoopes, C. 2002, AJ, 123, 142
Das, M., Boone, F., & Viallefond, F. 2010, A&A, 523, A63
Das, M., O'Neil, K., Vogel, S. N., & McGaugh, S. 2006, ApJ, 651, 853
Dekel, A., & Birnboim, Y. 2006, MNRAS, 368, 2
Dubinski, J., da Costa, L. N., Goldwirth, D. S., Lecar, M., & Piran, T. 1993, ApJ, 410, 458
Foster, C., & Nelson, L. A. 2009, ApJ, 699, 1252
Geller, M. J., & Huchra, J. P. 1989, Sci, 246, 897
Grogin, N. A., & Geller, M. J. 2000, AJ, 119, 32
Hahn, O., Porciani, C., Carollo, C. M., & Dekel, A. 2007, MNRAS, 375, 489
Helfer, T. T., Thornley, M. D., Regan, M. W., et al. 2003, ApJS, 145, 259
Hoyle, F., & Vogeley, M. S. 2004, ApJ, 607, 751
Icke, V. 1984, MNRAS, 206, 1P
Jester, S., Schneider, D. P., Richards, G. T., et al. 2005, AJ, 130, 873
Karachentseva, V. E., Karachentsev, I. D., & Richter, G. M. 1999, A&AS, 135, 221
Kennicutt, R. C., Jr. 1989, ApJ, 344, 685
Kennicutt, R. C., Jr. 1998, ApJ, 498, 541
Kereš, D., Katz, N., Weinberg, D. H., & Davé, R. 2005, MNRAS, 363, 2
Kirshner, R. P., Oemler, A., Jr., Schechter, P. L., & Shectman, S. A. 1981, ApJL, 248, L57
Kirshner, R. P., Oemler, A., Jr., Schechter, P. L., & Shectman, S. A. 1987, ApJ, 314, 493
Komatsu, E., Dunkley, J., Nolta, M. R., et al. 2009, ApJS, 180, 330
Kreckel, K., Croxall, K., Groves, B., van de Weygaert, R., & Pogge, R. W. 2015, ApJL, 798, L15
Kreckel, K., Platen, E., Aragón-Calvo, M. A., et al. 2011, AJ, 141, 4
Kreckel, K., Platen, E., Aragón-Calvo, M. A., et al. 2012, AJ, 144, 16
Leroy, A. K., Walter, F., Brinks, E., et al. 2008, AJ, 136, 2782
Makarov, D., Prugniel, P., Terekhova, N., Courtois, H., & Vauglin, I. 2014, A&A, 570, A13
Nakajima, T., Sakai, T., Asayama, S., et al. 2008, PASJ, 60, 435
Oke, J. B. 1990, AJ, 99, 1621
Peebles, P. J. E. 2001, ApJ, 557, 495
Peebles, P. J. E., & Nusser, A. 2010, Natur, 465, 565
Peimbert, M., & Torres-Peimbert, S. 1992, A&A, 253, 349
Penny, S. J., Brown, M. J. I., Pimbblet, K. A., et al. 2015, arXiv:1508.06186
Popescu, C. C., Hopp, U., Hagen, H. J., & Elsaesser, H. 1996, A&AS, 116, 43
Rahman, N., Howell, J. H., Helou, G., Mazzarella, J. M., & Buckalew, B. 2007, ApJ, 663, 908
Ricciardelli, E., Cava, A., Varela, J., & Quilis, V. 2014, MNRAS, 445, 4045
Rojas, R. R., Vogeley, M. S., Hoyle, F., & Brinkmann, J. 2004, ApJ, 617, 50
Sage, L. J., Weistrop, D., Cruzen, S., & Kompe, C. 1997, AJ, 114, 1753
Sahni, V., Sathyaprakah, B. S., & Shandarin, S. F. 1994, ApJ, 431, 20
Sakamoto, K., Okumura, S. K., Ishizuki, S., & Scoville, N. Z. 1999, ApJ, 525, 691
Sargsyan, L. A., & Weedman, D. W. 2009, ApJ, 701, 1398
Sellwood, J. A., & Wilkinson, A. 1993, RPPh, 56, 173
Sheth, R. K., & van de Weygaert, R. 2004, MNRAS, 350, 517
Silk, J., & Mamon, G. A. 2012, RAA, 12, 917
Soloman, P. M., & Vanden Bout, P. A. 2005, ARA&A, 43, 677
Stanonik, K., Platen, E., Aragón-Calvo, M. A., et al. 2009, ApJL, 696, L6
Sutter, P. M., Lavaux, G., Wandelt, B. D., & Weinberg, D. H. 2012, ApJ, 761, 44
Szomoru, A., van Gorkom, J. H., & Gregg, M. D. 1996, AJ, 111, 2141
Tully, R. B., Shaya, E. J., Karachentsev, I. D., et al. 2008, ApJ, 676, 184
van de Weygaert, R., Kreckel, K., Platen, E., et al. 2011, in Environment and the Formation of Galaxies: 30 years Later The Void Galaxy Survey, ed. I. Ferreras & A. Pasquali, 17
van de Weygaert, R., Platen, E., Tigrak, E., et al. 2010, in ASP Conf. Ser. 421, Galaxies in Isolation: Exploring Nature Versus Nurture, ed. L. Verdes-Montenegro, A. Del Olmo, & J. Sulentic (San Francisco, CA: ASP), 99
Waller, W. H. 1990, PASP, 102, 1217
Wegner, G., & Grogin, N. A. 2008, AJ, 136, 1
Weistrop, D., Hintzen, P., Liu, C., et al. 1995, AJ, 109, 981
Zel'dovich, Y. B. 1970, A&A, 5, 84